Momentum-transfer dependence of x-ray Raman scattering at the Be K-edge

C. Sternemann,[1] M. Volmer,[1] J. A. Soininen,[2,3] H. Nagasawa,[4] M. Paulus,[1] H. Enkisch,[1] G. Schmidt,[5] M. Tolan,[1] and W. Schülke[1]

[1]*Institute of Physics, University of Dortmund, D-44221 Dortmund, Germany*

[2]*Department of Physics, University of Washington, Seattle, Washington 98195, USA*

[3]*Optical Technology Division, National Institute of Standards and Technology, Gaithersburg, Maryland 20899, USA*

[4]*Faculty of Economics, Seikei University, Tokyo, 180-8633, Japan*

[5] *DELTA, University of Dortmund, D-44221 Dortmund, Germany*

(Received 3 February 2003; revised manuscript received 7 May 2003; published 17 July 2003)

Inelastic x-ray scattering spectra have been measured for energy losses around the Be K-edge in order to perform a systematic study of the dependence of the corresponding dynamic structure factor on both the absolute value and the direction of the momentum transfer. The measured x-ray Raman spectra show clear differences between spectra of different momentum transfer which are related to deviations from the dipole approximation of the x-ray Raman scattering cross section with increasing momentum transfer. In particular, the directional differences between x-ray Raman spectra for momentum transfer parallel and perpendicular to the *c* axis of single-crystal Be vanish completely at high momentum transfer. These results are attributed to monopole transitions of the excited electrons to *s*-type final states according to the results of a first-principles calculation which takes the particle-hole interaction into account. This theoretical approach is a valuable tool for modeling x-ray Raman spectra.

DOI: 10.1103/PhysRevB.68.035111 PACS number(s): 78.70.Ck, 71.15.−m, 71.20.−b, 71.45.Gm

I. INTRODUCTION

With the increasing availability of third-generation synchrotron sources nonresonant inelastic x-ray scattering from core excitations has become well established for measurements of the x-ray near-edge structure in low-Z materials. Generally, inelastic scattering experiments for investigation of core excitations can be performed utilizing electron energy-loss spectroscopy (EELS) (Ref. 1) or nonresonant inelastic x-ray scattering (NRIXS).[2] The inelastic scattering cross sections of both techniques are sensitive to the absolute value and the direction of the momentum transfer $\mathbf{q}$. Thus, anisotropies of the near-edge structure can be studied by changing the direction of the momentum transfer with respect to the crystallographic orientation of the sample.[3,4] Furthermore, excited states with different spatial symmetries can be probed by varying the magnitude of the momentum transfer,[5–8] which is not possible in standard x-ray absorption experiments. As long as one has $q \cdot a \ll 1$, where a is the electron orbital radius, the dipole allowed transitions dominate the excitation spectrum, whereas, for $q \cdot a \geqslant 1$, monopolar and higher-order transitions become more important. If the dipole approximation is valid, the cross section of an inelastic x-ray scattering experiment performed at an energy transfer close to a core electron binding energy is equivalent to that of x-ray absorption experiments with incident energies in the same energy regime. In the former case, the vector $\mathbf{q}$ of momentum transfer assumes the role, which the polarization vector $\boldsymbol{\epsilon}$ plays in x-ray absorption spectroscopy.[9,10]

Although EELS provides higher intensities compared to NRIXS and an energy resolution on the order of a few 0.1 eV, multiple scattering becomes a serious problem, especially if the magnitude of the momentum transfer is increased. Additionally, because of the surface sensitivity of EELS and soft-x-ray absorption, an ultrahigh vacuum sample environment is indispensable for these experiments. On the other hand NRIXS, also referred to as x-ray Raman scattering (XRS), is a pure bulk probe and is much less influenced by multiple-scattering effects.[11] This is the reason why it presents an important alternative for investigating the unoccupied density of states, local structure and chemistry of low-Z materials.[12] It also opens the possibility for measurements of x-ray Raman spectra of liquids and gases.[13,14]

Along with the experimental development of NRIXS, there has been a rapid improvement in its theoretical understanding.[15–20] An important ingredient of any calculation of core-excited states is to consider the influence of the core-hole left behind in the scattering process. In this work we utilize a first-principles calculation scheme[15,20] which was recently developed to solve this problem in connection with x-ray absorption and resonant inelastic x-ray scattering, and which can also be applied to x-ray Raman scattering.[8,20] Together with the calculations of the symmetry projected unoccupied density of states, these more advanced methods are very helpful in the interpretation of experimental results of core-excited states.

Nagasawa *et al.*[3] were the first to study the directional dependence of the x-ray Raman spectra of two simple metals, lithium and beryllium. They worked within the low-momentum-transfer regime ($q \cdot a \approx 0.35$) and observed strong anisotropies in the measurements of the Be K-edge for $\mathbf{q}$ perpendicular ($\mathbf{q} \| [100],[110]$) and parallel ($\mathbf{q} \| [001]$) to the *c* axis. On the contrary the measurements of the Li K-edge for $\mathbf{q} \| [100],[110]$, and [111] exhibited no anisotropy. This can be traced back to the fact that a Li crystal has a higher degree of symmetry than a Be crystal. A few years later, the x-ray Raman spectrum of the Li K-edge was measured as a function of the absolute value of momentum transfer,[6] showing a change in shape of the near edge struc-

ture with increasing q. Krisch *et al.*[7] performed similar measurements for $q\cdot a=0.176$ and $q\cdot a=1.95$, focusing on the near-edge structure of the Li K-edge up to 5 eV above the K-shell binding energy with a highly improved energy resolution of about 300 meV. In this study, the changes in the shape of the x-ray Raman spectra with increasing q have been attributed to the dominating contribution of monopolar transitions for high momentum transfer. A recent NRIXS study[8] of the momentum transfer dependence of the fluorine K-edge of LiF showed that a pre-edge peak in the spectra could be assigned to an *s*-type, i.e., dipole forbidden, exciton. The results of all these experimental studies have been successfully modeled utilizing a first principles scheme of treating the core hole interaction in the x-ray Raman scattering process.[19,20] Until now, to our knowledge, no combined theoretical and experimental study has been performed to examine the dependence of the cross section of nonresonant inelastic x-ray scattering from core electrons on both the magnitude and the direction of the momentum transfer $\mathbf{q}$. Since the application of XRS is becoming more popular in structural physics and chemistry,[12–14] it is the aim of the present study to investigate the directional anisotropies of the Be x-ray Raman spectra and their behavior by going beyond the dipole approximation. There are strong anisotropies in the x-ray Raman spectra of Be but their dependence on the magnitude of $\mathbf{q}$ has only been studied in a very early EELS measurement of Meixner *et al.*[21] (for $q\cdot a<1$). We performed a combined experimental and theoretical study of both the $|\mathbf{q}|$ and the $\mathbf{q}$ dependence of the Be K-edge x-ray Raman spectrum. We present results for a wide range of $q\cdot a$ values both for polycrystalline and single-crystal samples.

In what follows, a theoretical section reviews inelastic x-ray scattering from core excitations and the calculation scheme used to model the x-ray Raman spectra. Then the experimental results are presented and discussed with respect to the calculations. Finally, conclusions will be made.

II. CALCULATIONS

The quantity measured in an inelastic x-ray scattering experiment is the double differential cross section

$$\frac{d^2\sigma}{d\Omega d\omega}=\left(\frac{d\sigma}{d\Omega}\right)_{Th}S(\mathbf{q},\omega), \tag{2.1}$$

where $(d\sigma/d\Omega)_{Th}$ is the Thomson scattering cross section and $S(\mathbf{q},\omega)$ is the dynamic structure factor. The dynamic structure factor, a function of the momentum transfer $\mathbf{q}$ and the energy transfer ω, characterizes the possible excitation of the electron system. It can be expressed in terms of many-particle states as

$$S(\mathbf{q},\omega)=\sum_F\left|\left\langle F\left|\sum_l e^{i\mathbf{q}\cdot\mathbf{r}_l}\right|I\right\rangle\right|^2\delta(\omega+E_I-E_F), \tag{2.2}$$

where $|F\rangle$ is the final electron state with energy E_F, $|I\rangle$ is the initial electron state with energy E_I, and the sum l is over all electrons of the scattering system. Following Refs. 19 and 20, we approximate $S(\mathbf{q},\omega)$, when ω is close to a core binding energy, as

$$S(\mathbf{q},\omega)=-\frac{1}{\pi}\mathrm{Im}\left\langle 0\left|\hat{\rho}_{\mathbf{q}}\frac{1}{\omega-\hat{H}_{\mathrm{eff}}+i\gamma(\omega)}\hat{\rho}_{\mathbf{q}}^{\dagger}\right|0\right\rangle. \tag{2.3}$$

Here $\hat{H}_{\mathrm{eff}}$ is an approximate Hamiltonian of the excited system and $\gamma(\omega)$ accounts for the lifetime broadening of the spectrum. The state $|0\rangle$ denotes a Slater-determinant type of ground state wave function. The Fourier component of the density operator $\hat{\rho}_{\mathbf{q}}^{\dagger}$ can be expressed in second-quantized form

$$\hat{\rho}_{\mathbf{q}}^{\dagger}=\sum_{j,k}\langle\psi_j|e^{i\mathbf{q}\cdot\mathbf{r}}|\psi_k\rangle\hat{a}_j^{\dagger}\hat{a}_k, \tag{2.4}$$

where ψ_j and ψ_k are unoccupied and occupied single-particle states, respectively. The matrix elements in $\hat{\rho}_{\mathbf{q}}^{\dagger}$ account for the momentum-transfer dependence of the XRS spectra. On a qualitative level, the momentum-transfer dependence of XRS can most easily be understood by expanding the exponential in the matrix element as $\exp(i\mathbf{q}\cdot\mathbf{r})=1+i\mathbf{q}\cdot\mathbf{r}+(i\mathbf{q}\cdot\mathbf{r})^2/2+\cdots$. For low momentum transfers ($q\cdot a\ll 1$), the second term dominates, and mostly dipole allowed transitions are probed. When the momentum transfer is increased, other terms in the expansion become more important, giving the opportunity to study dipole-forbidden excitations. To get a quantitative result one has to consider also the spatial length scale of the final state and its dependence on the excitation energy. This can be done, for example, using a band-structure approach for the conduction electrons as is done in this work. Following Refs. 15,19 and 20, we approximate the excited state wave function with an electron-hole pair wave function. The electron-hole pair wave function is expressed in terms of conduction-band states $\psi_{n\mathbf{k}}$ and tight binding core states $\psi_{\mathbf{k}-\mathbf{q}\alpha}^{TB}$:

$$\Phi(\mathbf{r}_e,\mathbf{r}_h)=\sum_{n\mathbf{k}}C_{n\mathbf{k}}\psi_{n\mathbf{k}}(\mathbf{r}_e)[\psi_{\mathbf{k}-\mathbf{q}\alpha}^{TB}(\mathbf{r}_h)]^*,$$

where $C_{n\mathbf{k}}$ are the expansion coefficients. The atomic state of the core hole and its position in the unit cell are represented by the parameter α. The conduction-band wave functions $\psi_{n\mathbf{k}}$ are calculated using local-density approximation[22] pseudopotential[23] code and the core state is calculated using an atomic Hartree-Fock code. In the current approach, the effective Hamiltonian is

$$\hat{H}_{\mathrm{eff}}=\hat{H}_0+V_d+V_x.$$

The single particle term $\hat{H}_0$ is diagonal in the core hole-electron basis and the matrix elements are the differences between the energy of the core state and the electron single-particle states. The two electron-hole interaction terms account for the screened Coulomb interaction between the core hole and the electron V_d and a bare exchange interaction V_x. More information on the practical implementation of the current approach and examples of its application can be found

elsewhere.[8,15,19,20] The importance of the core hole-electron interaction in x-ray absorption and XRS calculations has been demonstrated for example in Refs. 15,17,16,19 and 20.

The numerical parameters used in this work are similar to the ones specified in Ref. 20 for Be. The only change is that here we have increased the number of conduction bands in the calculation to 60. This was done to obtain reliable results for spectra up to and beyond 80 eV above the edge. The numerical convergence of the calculated results with respect to the different numerical cutoffs is substantially better than the disagreement with the experiment. The theoretical approximations used in the calculations are the most important source of error, and here we will give a short overview of these approximations. In the current approach a quasiparticle approximation is used for both the electron and hole Green's functions. In a more general approach the full energy dependence of these Green's functions should be included (see, for example, Ref. 24). As explained in Ref. 19 the screening potential in V_d should be energy-dependent but it is approximated with a static potential in the current work. Also, the electron-hole interaction is assumed not to couple different hole states. As already mentioned the ground state wave function is approximated by a single Slater determinant and the excited state is approximated with electron-hole pair states. A more general approximation for both the ground and excited states might be needed in some systems. Additionally, phonon-electron interaction could play a role but it is not considered in this work. However, in the current approach the single-particle wave functions are solved in ground state configuration, which means that they can be solved with extremely high accuracy. Also, the approach is computationally efficient and has proven to be reliable in a range of materials.[8,19,20]

III. EXPERIMENT

The experiment was performed at the beamline SAW2 (BL9) of the Dortmund Electron Accelerator DELTA (Ref. 25) utilizing the standard setup for inelastic x-ray scattering spectroscopy which is described in detail elsewhere.[26] X rays supplied by the superconducting asymmetric wiggler are monochromatized using a Si(311) double crystal monochromator. The monochromatic beam is focused onto the sample by the saggitally bent second monochromator crystal, and the scattered radiation is analyzed by means of a spherically bent analyzer crystal using the Si(800) reflection at a fixed analyzer angle of 86° corresponding to an analyzer energy of 9.154 keV. By tuning the incident photon energy, the intensity of the scattered radiation is measured as a function of energy loss. The size of the polycrystalline Be sample is $20\times8\times2$ mm^3, and that of the Be single crystal $20\times8\times5$ mm^3, where the surfaces of the single crystal are oriented in [100] and [001] crystallographic directions. The measurements were carried out in transmission geometry for small scattering angles (low q) and in reflection geometry for large scattering angles (high q). We measured the Be K-edge spectra starting from the Be K electron binding energy of about 112.3 eV up to an energy transfer of 25 and 65 eV above the edge for the polycrystalline and single-crystal,

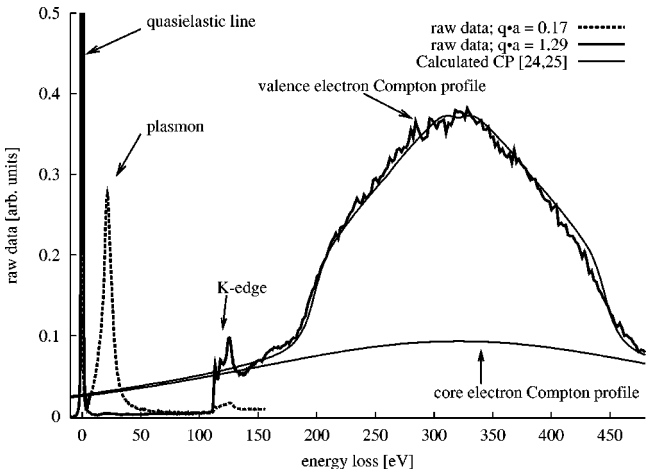

FIG. 1. Raw data presented for $q\cdot a=0.17$ and 1.29. Both spectra show the quasielastic line at 0 eV and the Be K-edge at 112.3 eV energy loss. For low $q\cdot a$ the plasmon excitation dominates the spectrum, whereas for high $q\cdot a$ the Compton profile appears. The total Compton profile and its core electron contribution calculated in Refs. 27 and 28 are also shown. The theoretical calculations were converted from a p_z scale to an energy-loss scale and fitted to the raw data by a scaling factor.

respectively. The momentum transfer q was chosen to be 1.21 and 9.03 Å^{-1} for both $\mathbf{q}||[100]$ (perpendicular to the c axis) and $\mathbf{q}||[001]$ (parallel to the c axis). For the polycrystalline sample, $q=2.40$ and 8.22 Å^{-1} were also measured. The absolute values of the momentum transfer correspond to values of $q\cdot a$ of 0.17, 0.34, 1.18, and 1.29 assuming the K-shell orbital radius $a=0.198$ Å. To reduce systematic errors, an average over several separate measurements was taken for each direction and each absolute value of $\mathbf{q}$. In addition, the plasmon and the particle-hole pair excitation spectra were measured for low q, whereas the Compton profile was measured for the high q values. These measurements, even if performed with lower statistical accuracy than the near-edge spectra, make it possible to normalize the K-edge spectra to absolute values using the f-sum rule.[6] In Fig. 1, such measurements are presented, showing the quasielastic line at 0 eV and the Be K-edge at 112.3 eV energy loss. For $q\cdot a=0.17$, the plasmon contribution to the total spectrum is presented, whereas, for $q\cdot a=1.29$, the Compton profile with its maximum around 320 eV appears. The total Compton profile[27] and its core electron contribution[28] calculated by Bansil and Kaprzyk are also given in Fig. 1. The calculated profiles were scaled to the experimental data.

The full width of half maximum of the quasielastic line indicates overall energy resolutions of 1.4 and 1.2 eV for the single-crystal and the polycrystalline measurements, respectively. A total of 10^4 counts is accumulated at the peak of the K-edge structure around 126 eV, corresponding to a standard uncertainty smaller than 1%. A linear background was subtracted from the raw data estimated from the count rate in the low-energy tail of the quasielastic line. Then the measured spectra were corrected for sample absorption, absorption of air and Kapton windows, efficiency of the ionization chamber used for the normalization of the data, and the energy

dependence ω_2/ω_1 of the scattering cross section. The changes introduced by these energy-dependent corrections are of the order of 1% over the energy range of interest.

The spectra of the polycrystalline sample for small q have been brought to an absolute scale applying the f-sum rule via

$$S(\mathbf{q},\omega)=\frac{\frac{\hbar q^2}{2m}}{\int_0^{\omega_c} I(\mathbf{q},\omega')\omega' d\omega'} I(\mathbf{q},\omega), \tag{3.1}$$

where $I(\mathbf{q},\omega)$ is the measured intensity after background subtraction and energy dependent corrections and ω_c is the energy of the Be K-edge at 112.3 eV. The valence electron contribution of the spectra within the energy-loss regime of the Be K-edge was found to be negligible by fitting an exponential to the tail of the valence electron excitation spectrum. For large q the normalization was performed using

$$S(\mathbf{q},\omega)=\frac{2\frac{\hbar q^2}{2m}-\int_{\omega_l}^{\omega_m} S_{CP}(\mathbf{q},\omega')\omega' d\omega'}{\int_0^{\omega_l} I(\mathbf{q},\omega')\omega' d\omega'} I(\mathbf{q},\omega), \tag{3.2}$$

where the factor 2 takes into account that the Compton profile is normalized to 2 valence and 2 core electrons. The experimental data $I(\mathbf{q},\omega)$ of the Compton profiles were taken up to an energy loss of $\omega_l=490$ eV. The calculated Compton profiles have been converted to the energy loss scale, $S_{CP}(\mathbf{q},\omega)$, and were integrated up to $\omega_m=2610$ eV, which corresponds to a p_z value of 15 a.u. These Compton profiles are obtained using the theoretical valence and core Compton profiles calculated in Refs. 27 and 28 for $p_z<5$ a.u., whereas the core Compton profiles for $p_z>5$ a.u. are free atomic Hartree-Fock Compton profiles.[29] Finally the contribution of the valence electron Compton profile underlying the Be K-edge spectra was subtracted utilizing the calculated valence electron Compton profiles. Because the Be K-edge for $q\cdot a=1.18$ was measured only up to 160 eV, this normalization procedure could not be applied. In this case, the subtraction of the valence electron contribution was obtained by scaling the calculated total Compton profile to the shape of the spectrum between 130 and 160 eV.

This procedure might be somewhat questionable, because the use of these theoretical Compton profiles presupposes the validity of the impulse approximation,[30,31] which is certainly violated in this range of energy transfer, especially in the case of the core contribution to the Compton profile. Moreover, violations of the impulse approximation even for the valence part of the Compton profile, because of final-state interactions[31–33] can give rise to uncertainties in the process of subtracting a calculated valence Compton profile. Nevertheless, this has no influence on the interpretation of the near-edge structures, because this problem applies in the range of energy losses higher than 150 eV, where the valence Compton profile starts a steeper rise.

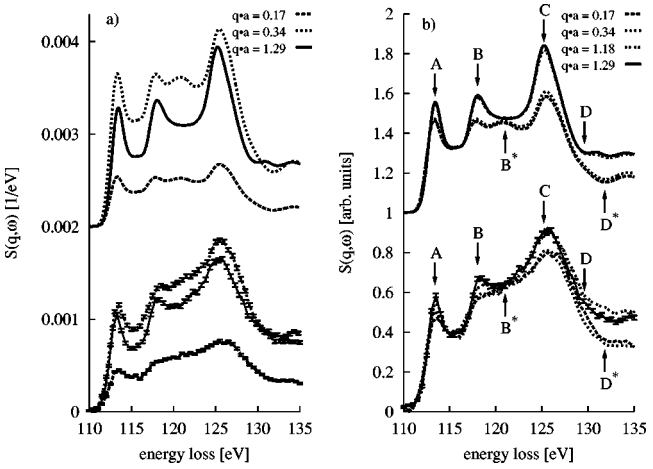

FIG. 2. (a) Experimental (lower part) and theoretical (upper part) Be K-edge spectra of the polycrystalline Be sample on an absolute scale $S(\mathbf{q},\omega)$ [1/eV]). The $q\cdot a$ values are indicated in the figure, and the calculated spectra are shifted vertically by 0.002 units. The experimental spectra are presented with error bars indicating the standard uncertainty. (b) Experimental (lower part) and theoretical (upper part) Be K-edge spectra of the polycrystalline Be sample on an arbitrary scale to allow a detailed discussion of the shape of the spectra. The calculated spectra are shifted vertically by 1. The identifiable features of the Be K-edge spectrum, denoted by A, B, B*, C, D, and D* are discussed within the text. The corresponding energy losses marked by the arrows are given in Table I.

IV. RESULTS AND DISCUSSION

First we will discuss the x-ray Raman scattering at the Be K-edge of the polycrystalline Be sample and its dependence on the absolute value of $\mathbf{q}$. The experimental and calculated Be K edges are presented in Fig. 2(a) as a function of energy and momentum transfer on an absolute scale. The theoretical calculations, which were obtained by the weighted average of the calculations for [100], [110], and [001] directions, are shifted vertically by 0.002 units. A good agreement between experiment and calculation is obtained both with respect to the overall shape and with respect to the absolute values of $S(\mathbf{q},\omega)$. The data for $q\cdot a=1.18$ are not presented, because of the lack of normalization in this case.

For a detailed discussion of the shape of the Be K-edge the spectra are scaled to their values at 116 eV energy loss and presented in Fig. 2(b). The main features of the Be K-edge spectra are denoted by A, B, B*, C, D, and D*, and their corresponding energy positions, marked by the arrows, are given in Table I. It should be realized that these features in the spectra represent transitions from a discrete core state to a continuum state, i.e., they generally do not represent transitions between discrete states. Additionally, the features are those of an electron-hole pair density of states, affected by the electron-hole interaction and so they are not necessarily directly related to features in the ground-state density of states. However, in some cases these two densities of states can be closely related, as we will soon show for the case of the Be K-edge. The identifiable features are labeled mostly to facilitate comparison between theory and experiment. The spectra measured at low momentum transfer, $q\cdot a=0.17$ and

TABLE I. Energy loss positions of the features A, B, B*, C, D, D*, E, and F marked by the corresponding arrows given as guide to the eye in Figs. 2–4. The values of the positions of A, B, B*, C, and D in the case of the single-crystal spectra are identical to the values given for the polycrystal measurement.

Polycrystalline sample						
Feature	A	B	B*	C	D	D*
Position (eV)	112.9	117.5	120.5	124.7	129.1	131.3
Single-crystal sample						
Feature				D*	E	F
$\mathbf{q}\|\|[100]$(eV)				131.6	137.5	158.5
$\mathbf{q}\|\|[001]$(eV)				131.6	137.5	159.5

0.34, for which the dipole approximation can be assumed to be valid exhibit two main peaks at A and C and a broad shoulder structure between B and C indicating a small peaklike structure at B*. The tail behind C clearly changes its slope at D*. These results are in good agreement with the results obtained by Nagasawa *et al.*[3] The Be K-edge measurements for $q\cdot a=1.18$ and 1.29 show clear differences compared to the spectra measured for $q\cdot a=0.17$ and 0.34. In addition to the features denoted by A and C, which gain more spectral weight with increasing q, a significant peak structure appears at B. The K-edge is now dominated by a three peak structure instead of a two peak and one shoulder structure as in the case of the low momentum transfers. Furthermore, the peak at C is shifted to a lower energy loss and a significant change in slope occurs at D. These apparent changes in the shape of the Be K-edge spectra with increasing momentum transfer have to be attributed to clear deviations from the dipole approximation as found also in the case of lithium.[6,7]

All these features and their momentum transfer dependence are present within the calculations of the x-ray Raman spectra, but the spectral weight of the peak height at C and the slope between B and C show small differences. Nevertheless, the overall agreement between experiment and calculation is remarkable. The calculation confirms, if the different excitation channels are separated with respect to the spatial symmetries (s,p,d) of the final state of the excited electron, that the shape of the Be K-edge is dominated by dipole-allowed transitions for small momentum transfers. On the contrary, the change in the shape of the Be K-edge for higher q can be assigned to the increasing contribution of transitions to *s*-type final states to the x-ray Raman scattering cross section. The contribution of transitions to *d*-type final states is indicated by the calculations to be negligible because of their small spectral weight. We study this in more detail by calculating the spectra for polycrystalline sample including only the dipole transitions or only the monopole transitions in the excitation matrix elements in Eq. (2.3). In Fig. 3 we show results for $q\cdot a=1.29$ of these two calculations together with the result when transitions $\Delta l\leqslant 2$ are allowed. Here the contribution of monopole transitions can be estimated to be 50 % of the total Be K-edge spectrum

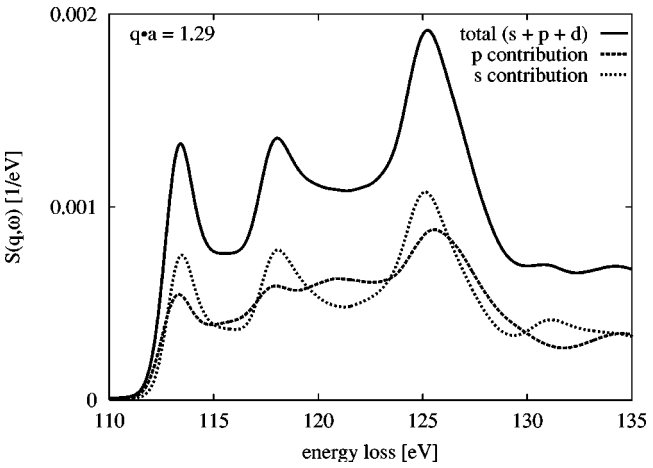

FIG. 3. Symmetry projected calculation of the Be K-edge spectra of the polycrystalline Be sample on an absolute scale for $q\cdot a=1.29$. The solid line represents the result of the full calculation including excitations into *s*-, *p*-, and *d*-type final states compared to calculations allowing only excitations into final states having *p* (long dashed) or *s* (short dashed) symmetry. The contribution of excitations into *d*-type final states is negligible within this energy loss range.

whereas the contribution of excitations into *d*-type final states is less than 1% within this energy range.

This interpretation is supported by calculations of the Be symmetry projected unoccupied density of states (DOS) of the ground state within a FLAPW (full potential augmented plane wave) scheme utilizing the WIEN97 package[34,35] shown in Fig. 4. The unoccupied DOS is presented as a function of the binding energy and the contribution of the *s*-DOS is magnified by a factor of 3. The arrows mark the same energy loss positions as in Fig. 2(b). The *s*-DOS exhibits three well pronounced peaks at positions A, B, and C compared to the

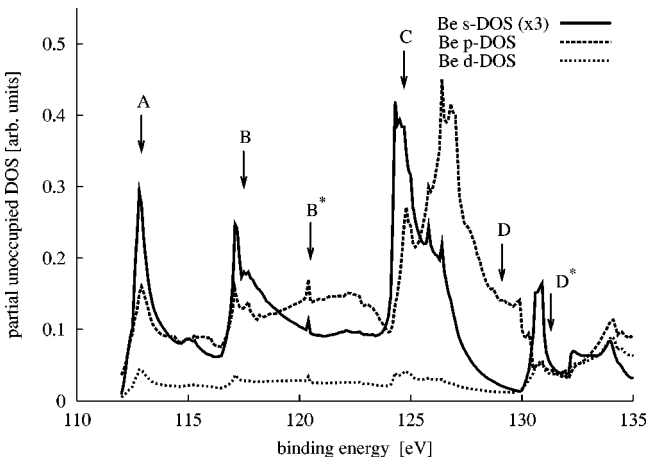

FIG. 4. Symmetry projected density of states (DOS) as a function of binding energy as calculated within the FLAPW scheme utilizing the WIEN97 package (Ref. 34). The arrows indicate the energy loss values of the features of the Be K-edge discussed in Fig. 2(b) denoted by A, B, B*, C, D, and D*. The *s*-DOS is multiplied by a factor of 3 to allow a better comparability between *s*- and p-DOS.

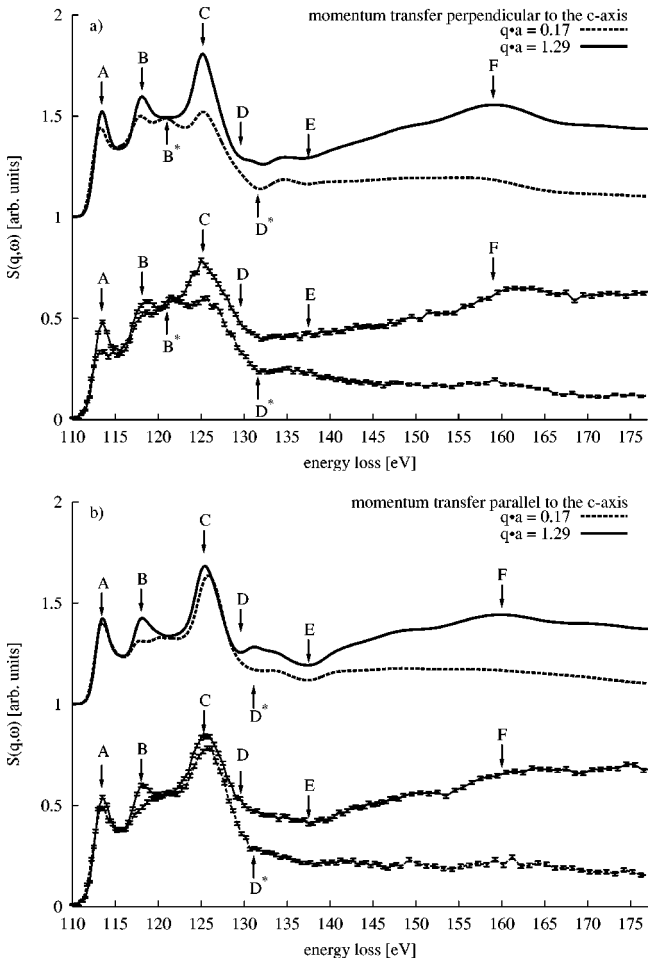

FIG. 5. (a) Experimental (lower part) and theoretical (upper part) Be K-edge spectra for $\mathbf{q}||[100]$ on an arbitrary scale. The $q \cdot a$ values are presented in the figure, and the calculated spectra are shifted vertically by 1. The error bars for the experimental spectra indicate the standard uncertainty. The identifiable features of the Be K-edge, denoted by A, B, B*, C, D, D*, E, and F are discussed in the text. The corresponding energy losses marked by the arrows are given in Table I. (b) Same as (a), but with momentum transfer $\mathbf{q}||[001]$.

p-DOS, in which the features A and B have smaller weight and the peak at C gives the dominating contribution and is shifted to higher energy losses with respect to the main peak of the *s*-DOS. Furthermore, the broad feature of the *p*-DOS ranging from 118 to 124 eV denoted by B* is not present in the *s*-DOS calculation. These differences in shape between the *p*- and *s*-DOS are in good agreement with the differences between Be K-edge spectra measured for low and high momentum transfers, which indicates that for $q \cdot a \geqslant 1$ the monopole transitions give an essential contribution to the x-ray Raman scattering cross section.

The momentum-transfer dependence with respect to both the absolute value of **q** and its orientation parallel or perpendicular to the *c* axis is subsequently discussed on the basis of the single-crystal measurements. The spectra measured for **q** parallel and perpendicular to the *c* axis up to an energy loss of 180 eV are presented in Figs. 5(a) and 5(b), respectively, and are compared to the corresponding calculations. The spectra are presented on an arbitrary scale, as is done for the polycrystalline results.

In the case of the low momentum transfer, $q \cdot a = 0.17$, a significant difference between the shape of the Be K-edge spectra for **q** parallel and perpendicular to the *c*-axis is present, which is in agreement with earlier measurements by Nagasawa *et al.*[3] The experimentally obtained results for $\mathbf{q}||[001]$ show two main peaks at A and C and a shoulder structure around B, whereas the measurement for $\mathbf{q}||[100]$ exhibits four smaller features around A, B, B*, and C. The change in slope at D* is identical for both measured crystallographic directions. Comparison with the calculated spectra yields a good agreement between experiment and calculation both for the distinct features between 112 and 135 eV energy loss, and also for the total shape of the K-edge up to 180 eV. Only the peak at A is smeared out in the experiment, and thus is slightly overestimated by the calculation. On the basis of the calculations, the x-ray Raman spectra for low momentum transfers presented here are well understood within the dipole approximation. The excitation to *p*-type final states dominates the scattering cross section.

The situation changes completely for the high momentum transfer regime with $q \cdot a = 1.29$. Both spectra show the typical three peak structure for energy losses close to the K-edge as found for the polycrystalline sample. The orientation dependence of the x-ray Raman spectra vanishes completely if energy losses up to 130 eV are considered. Minor directional differences are visible for higher energy losses corresponding to the shape of the spectra between D and F. The agreement between the theoretical calculations and the experimental data is very good. All features predicted by the calculations can be found in the experimental spectra except for the peak close to E for $\mathbf{q}||[100]$. In addition, the slopes of the spectra at energy losses above 160 eV differs between experiment and theory. This is most likely because of the uncertainty in subtracting the valence electron Compton profile from the experimental data, which starts to contribute significantly for energy losses above 150 eV as discussed above. Nevertheless, the Be K-edge spectra as a function of the direction and of the absolute value of the momentum transfer are quite accurately reproduced by the theoretical calculations. The vanishing of the directional differences for $q \cdot a = 1.29$ is traced back to the increasing contribution of *s*-type final states within the scattering process.

The changes in shape of the Be x-ray Raman spectra with increasing momentum transfer can be attributed to the changing weight of different symmetries contributing to the final state into which the electron is excited. In the high momentum transfer regime, where the dipole approximation cannot be applied, monopole transitions give a significant contribution to the scattering cross section. Because the calculations are able to give reliable predictions for $q \cdot a \geqslant 1$, not only can the unoccupied *p*-DOS ($q \cdot a \ll 1$) be tested by x-ray Raman measurements from a K-edge, but also the unoccupied *s*-DOS can be probed by measuring the Raman spectra for $q \cdot a \geqslant 1$. Thus this technique yields the possibility to easily distinguish excitations of different final state symmetries by performing measurements at a single absorption edge.

V. CONCLUSION

We studied the momentum-transfer dependence of the Be K-edge fine structure with respect to both the absolute value of the momentum transfer and its direction utilizing nonresonant x-ray Raman scattering. The experimental results are compared with calculations modeling the x-ray Raman spectra including core-hole effects. The fine structures, the overall shape and the absolute values of the spectra show good overall agreement between experiment and theory. For low momentum transfer, the shape of the Be K-edge is mainly due to contributions from dipole-allowed transitions. When the momentum transfer is increased, monopolar transitions to *s*-type final states give a significant contribution to the scattering cross section. It was shown that for high momentum transfer the directional differences in the spectra for **q** parallel and perpendicular to the *c* axis vanish, which is traced back to the mixing of the different spatial symmetries.

ACKNOWLEDGMENTS

This work was supported by the German Federal Ministry of Education and Research under Contract No. 05 ET9 PEA. J. A. S. was supported in part by the U. S. Department of Energy through Grant No. DE-FG03-97ER45623 and the National Institute of Standards and Technology, all through the Computational Materials Science Network (CMSN). The authors would like to thank A. Bansil and S. Kaprzyk for giving the LDA Be Compton profiles in numerical form. We thank the DELTA machine group for providing the excellent beam conditions during the measurements. DELTA is founded by the Land Nordrhein-Westfalen and the University of Dortmund. The support of DELTA by the Forschungszentrum Jülich is gratefully acknowledged.

[1] J.J. Ritsko, S.E. Schnatterly, and P.C. Gibbons, Phys. Rev. B **10**, 5017 (1974).
[2] S. Doniach, P.M. Platzman, and J.T. Yue, Phys. Rev. B **4**, 3345 (1971).
[3] H. Nagasawa, S. Mourikis, and W. Schülke, J. Phys. Soc. Jpn. **58**, 710 (1989).
[4] N. Watanabe, H. Hayashi, Y. Udagawa, K. Takeshita, and H. Kawata, Appl. Phys. Lett. **69**, 1370 (1996).
[5] J.M. Auerhammer and P. Rez, Phys. Rev. B **40**, 2024 (1989).
[6] H. Nagasawa, S. Mourikis, and W. Schülke, J. Phys. Soc. Jpn. **66**, 3139 (1997).
[7] M.H. Krisch, F. Sette, C. Masciovecchio, and R. Verbeni, Phys. Rev. Lett. **78**, 2843 (1997).
[8] K. Hämäläinen, S. Galambosi, J.A. Soininen, E.L. Shirley, J.-P. Rueff, and A. Shukla, Phys. Rev. B **65**, 155111 (2002).
[9] Y. Mizuno and Y. Ohmura, J. Phys. Soc. Jpn. **22**, 445 (1967).
[10] T. Suzuki, J. Phys. Soc. Jpn. **22**, 1139 (1967).
[11] J. Felsteiner and W. Schülke, Nucl. Instrum. Methods Phys. Res. A **132**, 1 (1997).
[12] U. Bergmann, P. Glatzel, and S.P. Cramer, Microchem. J. **71**, 221 (2002).
[13] D.T. Bowron, M.H. Krisch, A.C. Barnes, J.L. Finney, A. Kaprolat, and M. Lorenzen, Phys. Rev. B **62**, 9223 (2000).
[14] U. Bergmann, Ph. Wernet, P. Glatzel, M. Cavalleri, L.G.M. Pettersson, A. Nilsson, and S.P. Cramer, Phys. Rev. B **66**, 092107 (2002).
[15] E.L. Shirley, Phys. Rev. Lett. **80**, 794 (1998).
[16] J.J. Rehr and R.C. Albers, Rev. Mod. Phys. **72**, 621 (2000).
[17] T. Mizoguchi, I. Tanaka, M. Yoshiya, F. Oba, K. Ogasawara, and H. Adachi, Phys. Rev. B **61**, 2180 (2000).
[18] J.A. Soininen and E.L. Shirley, Phys. Rev. B **61**, 16 423 (2000).
[19] J.A. Soininen, K. Hämäläinen, W.A. Caliebe, C.-C. Kao, and E.L. Shirley, J. Phys.: Condens. Matter **13**, 8039 (2001).
[20] J.A. Soininen and E.L. Shirley, Phys. Rev. B **64**, 165112 (2001).
[21] A.E. Meixner, M. Schlüter, P.M. Platzman, and G.S. Brown, Phys. Rev. B **17**, 686 (1978).
[22] P. Hohenberg and W. Kohn, Phys. Rev. **136**, 864 (1964); W. Kohn and L.J. Sham, *ibid.* **140**, 1133 (1965).
[23] For a review, see W.E. Pickett, Comput. Phys. Rep. **9**, 115 (1989).
[24] L. Campbell, L. Hedin, J.J. Rehr, and W. Bardyszewski, Phys. Rev. B **65**, 064107 (2002).
[25] Dortmund Electron Accelerator (DELTA), University of Dortmund, Maria-Goeppert-Mayer-Str. 2, D-44221 Dortmund, Germany (www.delta.uni-dortmund.de).
[26] A. Berthold, S. Mourikis, J.R. Schmitz, W. Schülke, and H. Schulte-Schrepping, Nucl. Instrum. Methods Phys. Res. A **317**, 373 (1992).
[27] S. Huotari, K. Hämäläinen, S. Manninen, S. Kaprzyk, A. Bansil, W. Caliebe, T. Buslaps, V. Honkimäki, and P. Suortti, Phys. Rev. B **62**, 7956 (2000).
[28] A. Bansil and S. Kaprzyk (private communication).
[29] F. Biggs, L.B. Mendelsohn, and J.B. Mann, At. Data Nucl. Data Tables **16**, 201 (1975).
[30] P. Eisenberger and P.M. Platzman, Phys. Rev. A **2**, 415 (1970).
[31] S. Huotari, K. Hämäläinen, S. Manninen, M. Marangolo, and A. Issolah, J. Phys. Chem. Solids **62**, 2205 (2001).
[32] C. Sternemann, K. Hämäläinen, A. Kaprolat, A. Soininen, G. Döring, C.-C. Kao, S. Manninen, and W. Schülke, Phys. Rev. B **62**, R7687 (2000).
[33] J.A. Soininen, K. Hämäläinen, and S. Manninen, Phys. Rev. B **64**, 125116 (2001).
[34] P. Blaha, K. Schwarz, J. Luitz, WIEN 97, Vienna University of Technology, Wien 1997; update of P. Blaha, K. Schwarz, P. Sorantin, and S.B. Trickey, Comput. Phys. Commun. **59**, 399 (1990).
[35] The use of WIEN97 in this work does not constitute an endorsement or certification by the National Institute of Standards and Technology.